Stochastic models for the space-time evolution of martensitic avalanches

Pierluigi Cesana

Institute of Mathematics for Industry
Kyushu University, Japan

Hysteresis, Avalanches and Interfaces in Solid Phase Transformations
20$^{\mathrm{th}}$ September, 2016

Overview

- General Branching Random Walk model for martensitic avalanches
- Fragmentation model (SOC à-la-Bak) for the crystal variants of an elastic crystal

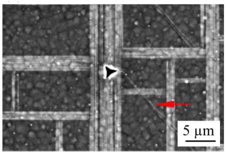

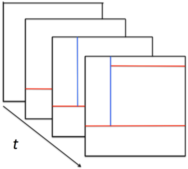

Niemann et al. APL Mater. 4, 064101 (2016)

- Joint work with John Ball and Ben Hambly (Oxford)
  - J. Ball, P.C., B. Hambly, Proceedings ESOMAT15
  - P.C., B. Hambly, in progress
  - P.C., M. Porta, T. Lookman, JMPS 2014
  - S. Patching, P.C, A. Rueland, in preparation

Martensitic transformation

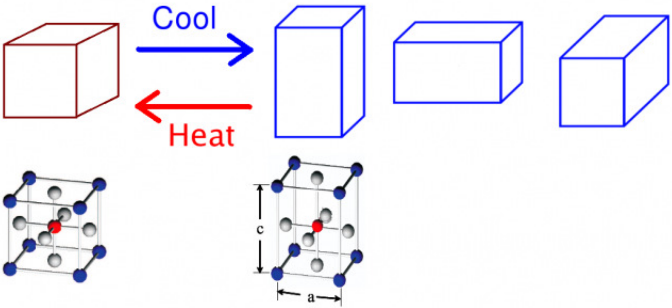

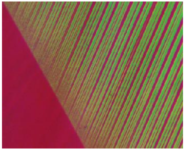

Aus-Mar interface, C.Chu

Elasticity framework

- $F \in \mathbb{R}^{3\times 3}$ the deformation gradient
- $\psi(F)$ the free-energy density

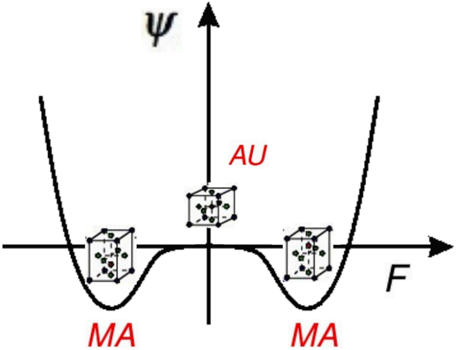

Figure : First-order phase transition, fixed temperature

Effect of temperature

- $F \in \mathbb{R}^{3\times 3}$ the deformation gradient
- $\psi(\theta; F)$ the free-energy density

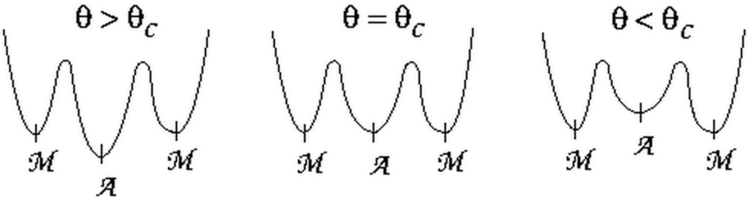

Courtesy Tim Duerig

Self-similarity

Transformed sample of Cu-Zn-Al (after cooling). Optical microscope with polarized light 3mm x 2mm (Morin)

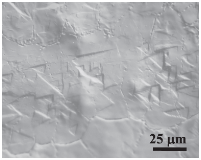

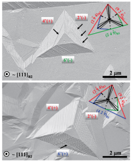

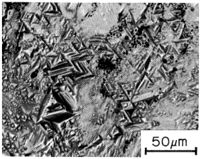

LEFT-CENTER: SEM micrograph pictures, Ti-Ni;
RIGHT: Ti-Ni-Cu (orthorombic martensite), self-acc.

M. Nishida et al. (2012) Self-accommodation of B19 martensite in Ti-Ni shape memory alloys-Part 1. Morphological and crystallographic studies of the variant selection rule, Philosophical Magazine, 92:17, 2215-2233.

Martensitic transformation

A martensitic transformation is a phase transition which involves a cooperative motion of a set of atoms across an interface causing a shape change and a sound.

Philip C. Clapp, ICOMAT95

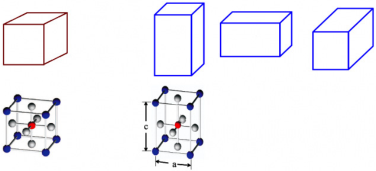

Avalanches

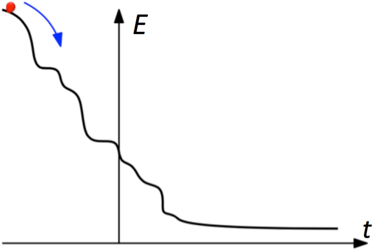

- intermittent evolution as a sequence of jerks (avalanches)
- athermal behavior
- jerky behavior is consequence of **disorder**

Acoustic emissions

- Avalanches detected by ultrasonic AEs

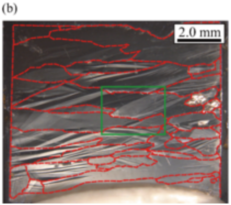

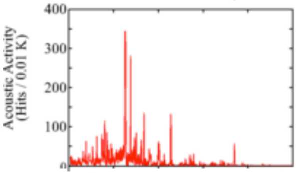

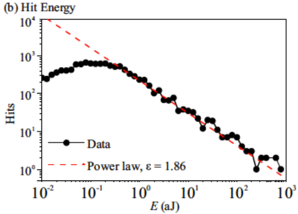

1) Polarized light optical micrograph of sample of martensitic NiMnGa at room temperature.
2) Emission hits per 0.01K temperature interval (acoustic activity).
3) Histogram of the number of hits vs the absolute energy.

Niemann et al. (2014), PRB

Universality

Universality class critical exponents α and ϵ and variant-multiplicity for systems transforming from cubic to selected martensitic symmetries. They are estimated as averaged values in the adiabatic limit. For monoclinic martensites, data reported for Cu–Al–Zn, Cu–Al–Be, Cu–Al–Mn [23] and Ni–Al [24] have been used. For orthorhombic martensite data are from two Cu-Al-Ni [23] and from a Cu-Al-Mn alloy [17]. For tetragonal martensite data from single- and poly-crystalline Fe-Pd have been used [27].

M-symmetry	α	ϵ	Multiplicity
Monoclinic	3.0 ± 0.2	2.0 ± 0.2	12
Orthorhombic	2.4 ± 0.1	–	6
Tetragonal	2.0 ± 0.3	1.6 ± 0.1	3

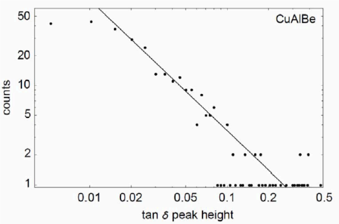

- A. Planes et al. (2013) *Acoustic emission in martensitic transformations*, Journal of Alloys and Compounds, 577S S699-S704

- E. Salje et al. (2009) *Jerky elasticity: Avalanches and the martensitic transition in shape-memory alloys*, APL 95

Fragmentation

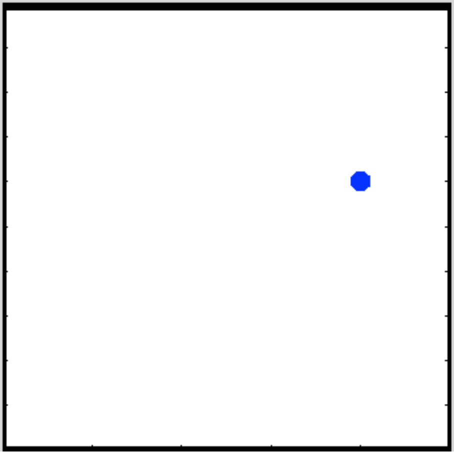

Fragmentation

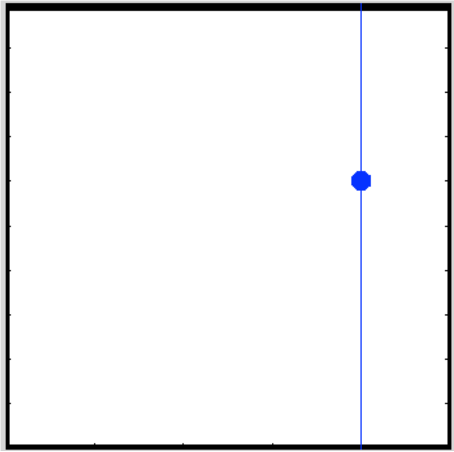

Fragmentation

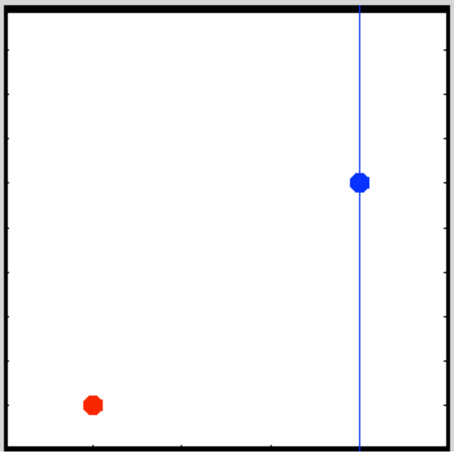

Fragmentation

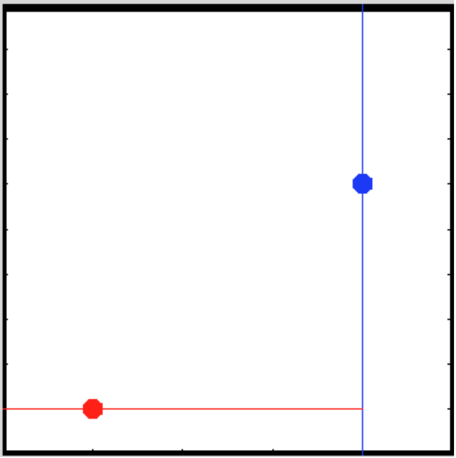

Fragmentation

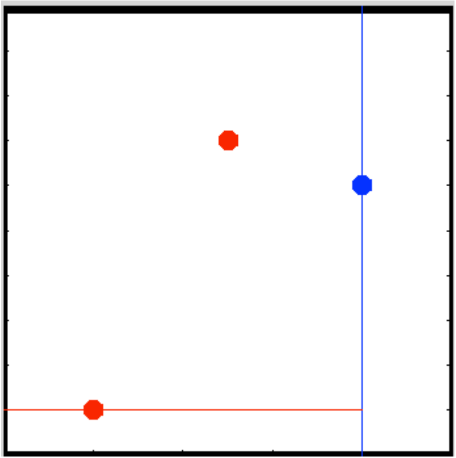

Fragmentation

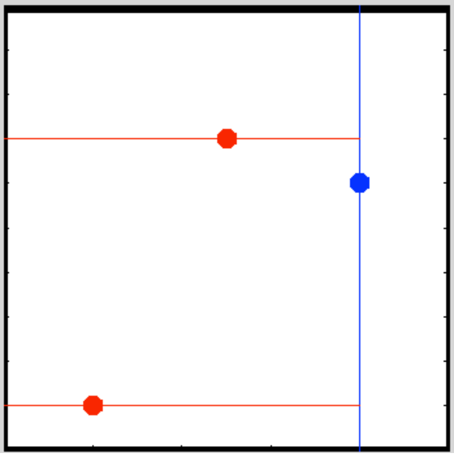

n=100

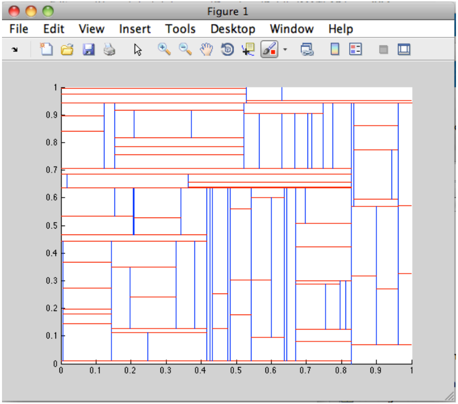
Figure 1
File Edit View Insert Tools Desktop Window Help
1
0.9
0.8
0.7
0.6
0.5
0.4
0.3
0.2
0.1
0
0 0.1 0.2 0.3 0.4 0.5 0.6 0.7 0.8 0.9 1

n=1000

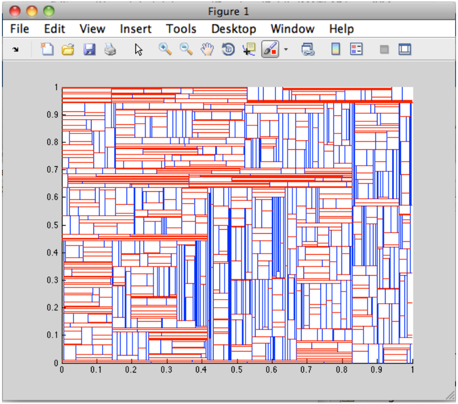
Figure 1
File Edit View Insert Tools Desktop Window Help
0
0.1
0.2
0.3
0.4
0.5
0.6
0.7
0.8
0.9
1

n=5000

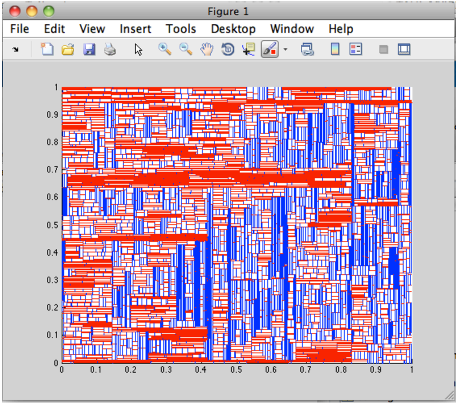
Figure 1
File Edit View Insert Tools Desktop Window Help
1
0.9
0.8
0.7
0.6
0.5
0.4
0.3
0.2
0.1
0
0 0.1 0.2 0.3 0.4 0.5 0.6 0.7 0.8 0.9 1

SEM micrograph (backscattered electron contrast) of an epitaxial Ni-Mn-Ga film in the martensitic state at room temperature. (b) A zoom-in shows two different microstructures. All contrast comes from mesoscopic twin boundaries. (c, d) TEM micrographs at cross-sections along the lines marked in (b).

R. Niemannet al. (2014) PRB

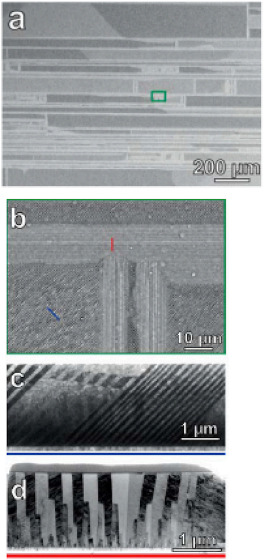

3, 4 Phases

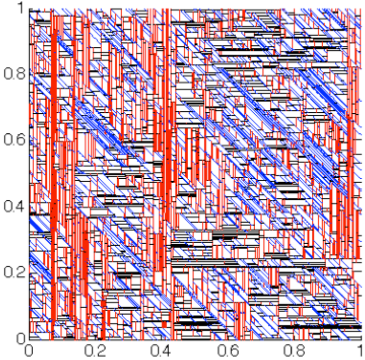

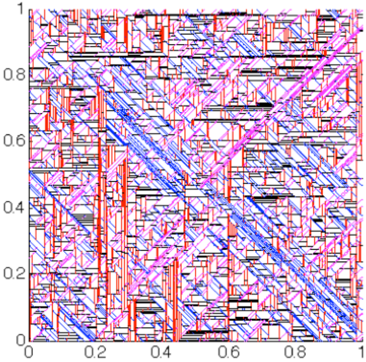

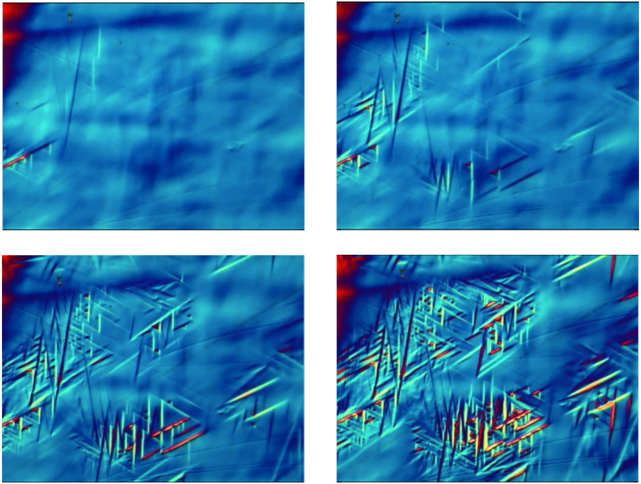

Avalanche formation of a habit plane variant cluster with triangular morphology in TiNbAl [Kamioka, ...,T. Inamura, Proceedings of ESOMAT 2015]

6 Phases

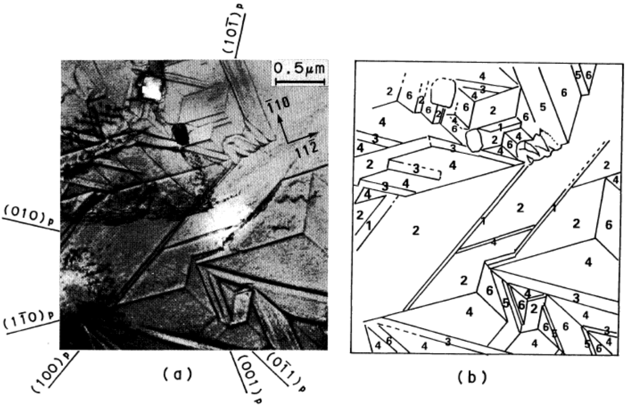

Fig. 9 (a) Configuration of six variants. Surface marking on the surface of the parent phase (electron micrograph).
(b) Schematic explanation of (a).

Self-accomodation structure in Ti-Ni-Cu Orthorombic Martensite, Watanabe et al., J. Japan Inst. Metals, 54, N.8 1990.

Other shapes

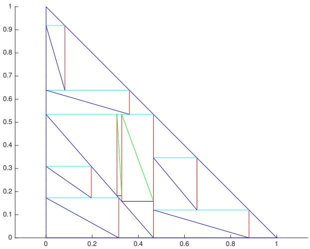

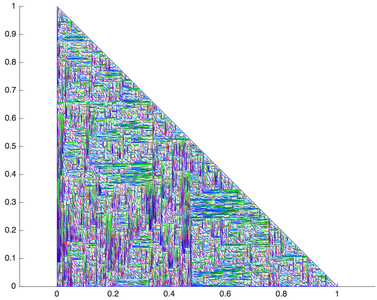

The fragmentation model

- Pick a point at random (nucleation)

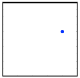

- Choose a direction, V (with probability p) or H

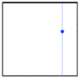

- The general rectangle (a, b) splits into

$$(a,b) \to \begin{cases} (aU, b), (a(1-U), b) \ \textit{with probability} \ \mathrm{p} \\ (a, bU), (a, b(1-U)) \ \textit{with probability} \ 1\text{-}\mathrm{p} \end{cases}$$

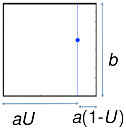

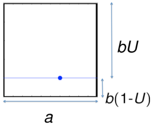

General Branching Random Walk

- The whole structure can be captured in a tree as the evolution inside any rectangle does not affect what happens outside that rectangle.

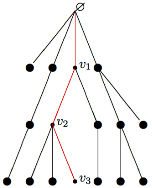

- Thus in our tree each vertex will represent a rectangle .
- We use some results from Biggins[1]: super-critical GBRW have a shape theorem indicating the region where the number of particles will grow exponentially.

[1] How fast does a general branching random walk spread? *IMA Vol. Math. Appl., 84, Springer, New York, 1997*.

$-\log$ transformation

- Transformation:

$$\begin{aligned} x &= -\log a \quad &\geq 0 \\ y &= -\log b \quad &\geq 0 \end{aligned}$$

- Each rectangle is an individual in the branching process and location is determined by its sides $\to$ GBRW in $\mathbb{R}^2_+$.
- Ancestor $(0,1) \times (0,1) \to (0,0)$
- The smaller the rectangles, the larger the coordinates

Constructing the tree

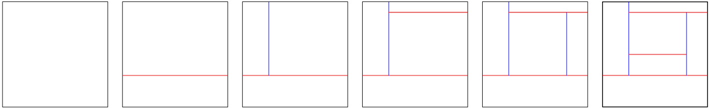

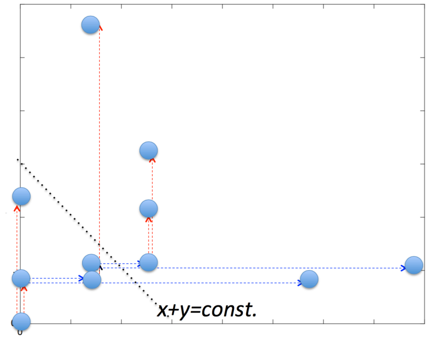

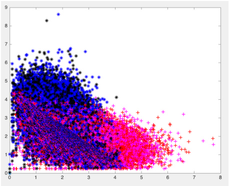

Branching Random Walk

- In Crump-Mode-Jagers (General Branching Process) model an individual z:
  - is born at time $\sigma_z \geq 0$,
  - has a lifetime $L_z \geq 0$,
  - has offspring whose birth times are determined by a point process ξ_z on $(0, \infty)$.
- For a General Branching Random Walk we include a point process for the birth position η_z (as well as birth times).

General Branching Random Walk

- Let the Bernoulli r.v. $B_i = \begin{cases} 0 & \textit{horizontal} \quad 1-p \\ 1 & \textit{vertical} \quad p \end{cases}$
- Let U_i uniform r.v. in $[0, 1]$
- Outcomes of the general rectangle (a, b) are

$$(a, b) \to \begin{cases} \Big(B_i U_i a,\ (1 - B_i) U_i b\Big) \\ \\ \Big(B_i (1 - U_i) a,\ (1 - B_i)(1 - U_i) b\Big) \end{cases}$$

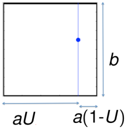

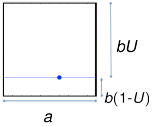

General Branching Random Walk

- Birth time: proportional to $-\log(Area)$ of rectangle splitting
- $(\eta_i, \xi_i) =$ space,time position of offspring of i

$$\eta_i, \xi_i = \begin{cases} (-B_i \log U_i, -(1-B_i) \log U_i) & -\log U_i \\ (-B_i \log(1-U_i), -(1-B_i) \log(1-U_i)) & -\log(1-U_i) \end{cases}$$

- The space-time point process:

$$(\eta(d\mathbf{x}), \xi(dt)) = \begin{cases} (\delta_{(-\log u, 0)}(d\mathbf{x}), \delta_{-\log t}(dt)) I_{\{u=t\}} + \\ (\delta_{(-\log(1-u), 0)}(d\mathbf{x}), \delta_{-\log(1-t)}(dt)) I_{\{u=t\}} & 1/2 \\ \\ (\delta_{(0, -\log u)}(d\mathbf{x}), \delta_{-\log t}(dt)) I_{\{u=t\}} + \\ (\delta_{(0, -\log(1-u))}(d\mathbf{x}), \delta_{-\log(1-t)}(dt)) I_{\{u=t\}} & 1/2 \end{cases}$$

- birth time of $\sigma_\emptyset = 0$
- birth time of $\sigma_{ij} = \sigma_i + \inf\{t : \xi_i(t) \geq j\}$

Time

- $t = -log(1 - U_1) - log(1 - U_2) - log(1 - U_3)$
- Largest area is $(1 - U_1)(1 - U_2)(1 - U_3)$
- That is $t = -log(Area)$
- at time t largest area is e^{-t}

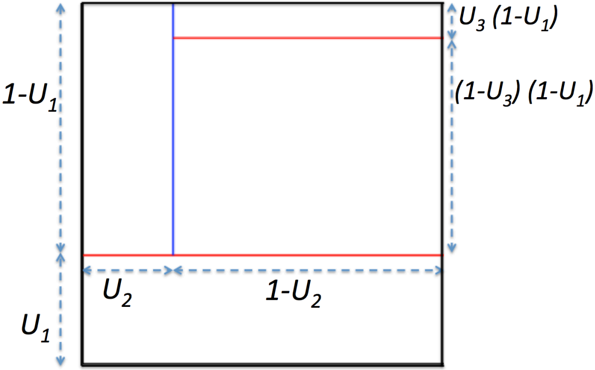

Shape Theorem

• We want to keep track of $N_t(A) = \#$ individuals in the set A at time t.

Take $A \subset \mathbb{R}^2_+$ closed, convex, non-empty interior.

1. If $A \cap \{(x, y) : x + y = 1\} = \emptyset$ then
$$t^{-1} \log N_t(tA) \to -\infty \qquad t \to \infty, a.s.$$
2. If $A \cap \{(x, y) : x + y = 1\} \neq \emptyset$ then
$$t^{-1} \log N_t(tA) \to \beta \geq 0 \qquad t \to \infty, a.s.$$

where

- $\beta = \sup\{\alpha^*(a) : a \in A\}$
- $\alpha^*(\mathbf{a}) = \inf_{\mathbf{w}}\{\mathbf{a} \cdot \mathbf{w} + \alpha(\mathbf{w})\}$
- $\alpha(\mathbf{a}) = \inf\{\phi : m(\mathbf{w}, \phi) \leq 1\}$
- $$m(\mathbf{w}, \phi) = E \int e^{-\mathbf{w} \cdot \mathbf{x} - \phi t} \eta_\emptyset(d\mathbf{x}) \xi_\emptyset(dt), \qquad \mathbf{w} \in \mathbb{R}^2, \phi \in \mathbb{R}_+.$$

  the moment-generating function for the position and birth times of offsprings.

Interpretation

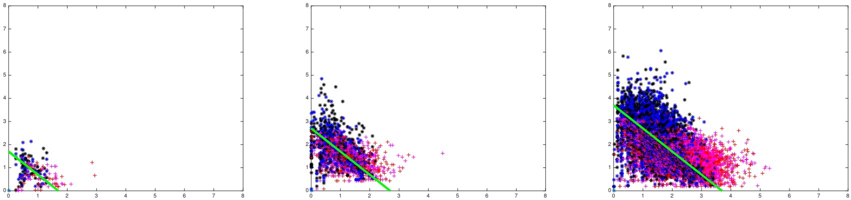

Figure : $n = 10^2, 10^3, 10^4$

The line $x + y = t$
Areas $\sim e^{-t}$

Application

- At time t largest Area=e^{-t} $\rightarrow$ $t = -\log Area$
- Shape theorem describes exponential growth of individuals N in a certain set $A \subset \mathbb{R}^2_{++}$

$$\lim_{t\to\infty} t^{-1} \log(t\, N_t(A)) = \beta \geq 0$$

- for finite t, approximation formula

$$N_t(A_{x,y}) = e^{t\, f(\frac{x}{t},\frac{y}{t})}$$

with:

$$f\left(\frac{x}{t},\frac{y}{t}\right) = \begin{cases} \sqrt{1-(2p-1)^2}\sqrt{1-(\frac{x}{t}-\frac{y}{t})^2}+ & \\ \qquad +(1-2p)(\frac{x}{t}-\frac{y}{t}) & \text{if } \frac{x}{t}+\frac{y}{t}=1 \\ -\infty & \text{if } \frac{x}{t}+\frac{y}{t}\neq 1 \end{cases}$$

Numerical results (rectangles)

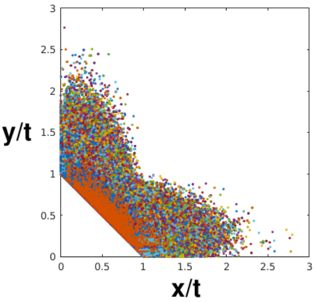

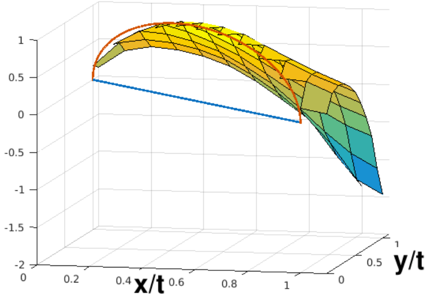

- for $p = \frac{1}{2}$, $n = 2000$, $t \approx 6.9$
- Analytical solution

$$f(\tfrac{x}{t}, 1 - \tfrac{x}{t}) = 2\sqrt{\tfrac{x}{t}(1 - \tfrac{x}{t})}$$

holds on the line $\frac{x}{t} + \frac{y}{t} = 1$ $\quad (ab = e^{-t})$

Numerical results (interfaces)

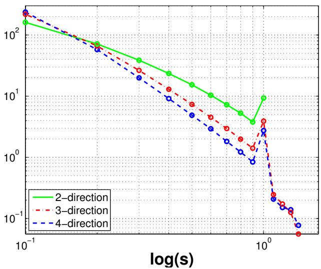

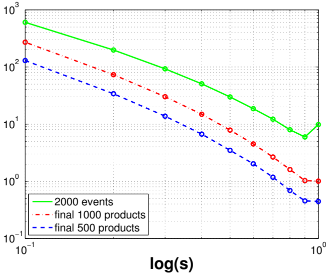

M-symmetry	α	ϵ	Multiplicity
Monoclinic	3.0 ± 0.2	2.0 ± 0.2	12
Orthorhombic	2.4 ± 0.1	–	6
Tetragonal	2.0 ± 0.3	1.6 ± 0.1	3

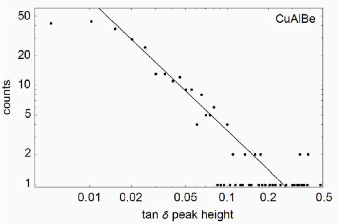

Salje et al. (2009) *Jerky elasticity: Avalanches and the martensitic transition in shape-memory alloy*, APL 95

Case with bias

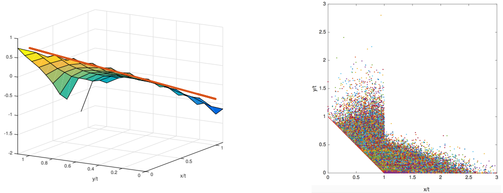

Figure : Histograms, $p = 0.1$

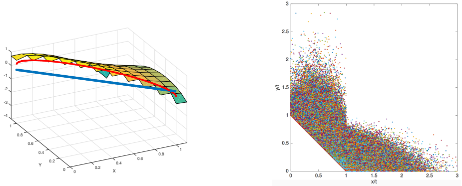

Figure : Histograms, $p = 0.3$

Mondrian process

The Mondrian Process, D. M. Roy, Y. W. Teh, Advances in Neural Information Processing Systems 21 (NIPS 2008)

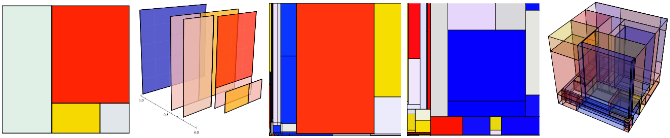

- Initial budget $\lambda > 0$
- Nucleus picked at random
- Cut is made with probability proportional to its length
- Cost of cut $\propto$ its length
- Arrest when the total length reaches the budget

Fractal microstructure

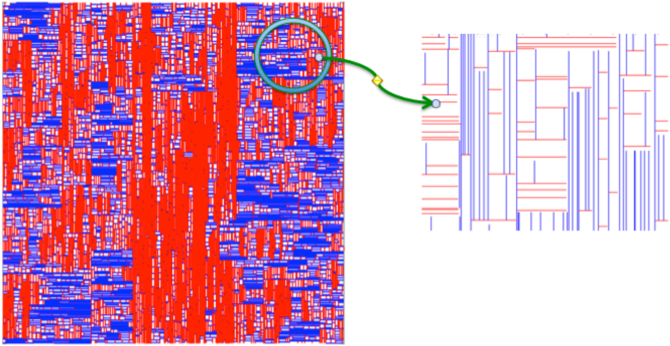

3D model

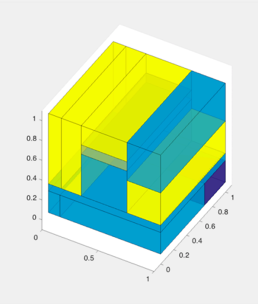

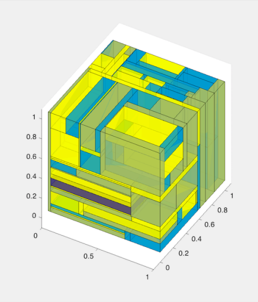

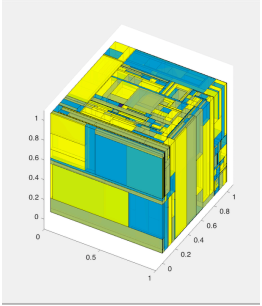

$n = 10, 10^2, 10^3$ events.

3D model

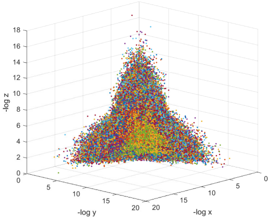

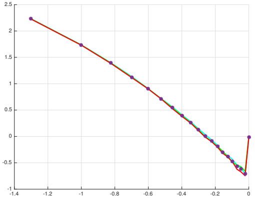

Cloud and plate distribution.

Random angles

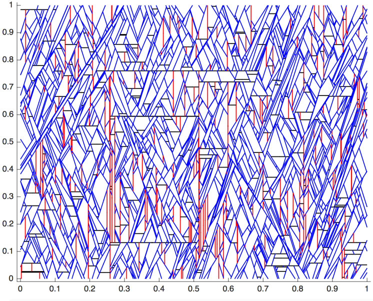

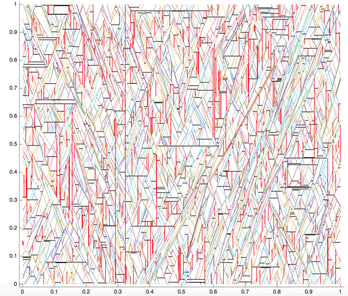

- Surface energy
- Unpinning strategy (joint w. A. Collevecchio, Monash)

TIVP model

G. Torrents et al., Geometrical model for martensitic phase transitions: understanding criticality and weak universality during microstructure growth, to appear

- discrete model
- our focus on new individuals
- discrete features

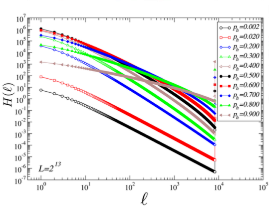

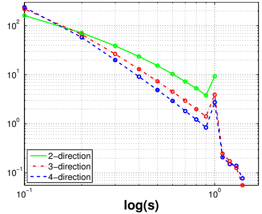

- statistics for interfaces and areas

Self-similar nested microstructure

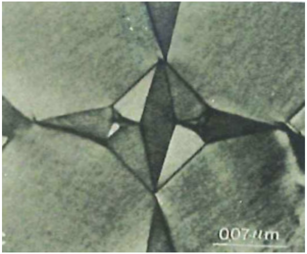

Figure : Star disclination in $Pb_3(VO_4)_2$ *(HREM)*, C. Manolikas, S. Amelinckx, Phys. Stat. Sol. 1980.

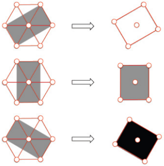

Figure : The 2D version of the hexagonal-to-orthorhombic transformation (Mg-Cd, $Mg_2Al_4Si_5O_{18}$) is the triangle-to-centered-rectangle (TR) transformation.

Exact solutions

$$\bullet \Psi(F) \leftarrow \min_{F \in \mathbb{R}^{3\times 3}} + \textit{Kinematic Compatibility}$$

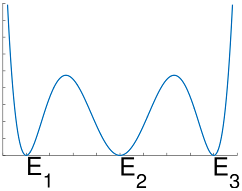

- To find a deformation field $y : \Omega :\to \mathbb{R}^3$ s.t.

$$\nabla y \in \{E_1, E_2, E_3\}$$

and y is Hölder continuous.

Kinematic compatibility (KC)

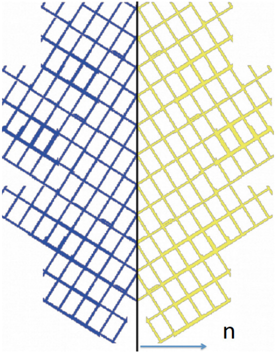

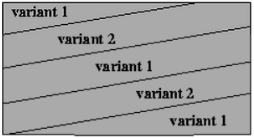

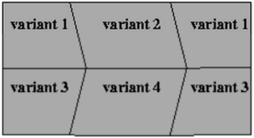

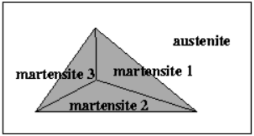

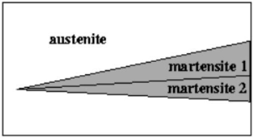

$F_1 = \nabla y_1 \qquad F_2 = \nabla y_2$

Conservation of tangential component of $\nabla y_1, \nabla y_2 \rightarrow F_1 - F_2 = a \otimes n$

Kinematic compatibility

$$y : \Omega \to \mathbb{R}^3 : \nabla y \in \{E_1, E_2, E_3\}$$

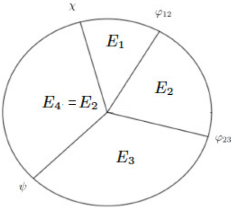

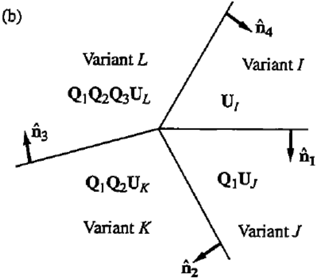

1. $\mathbf{Q}_1\mathbf{U}_J - \mathbf{U}_I = \mathbf{b}_1 \otimes \hat{\mathbf{n}}_1$
2. $\mathbf{Q}_1\mathbf{Q}_2\mathbf{U}_K - \mathbf{Q}_1\mathbf{U}_J = \mathbf{b}_2 \otimes \hat{\mathbf{n}}_2$
3. $\mathbf{Q}_1\mathbf{Q}_2\mathbf{Q}_3\mathbf{U}_L - \mathbf{Q}_1\mathbf{Q}_2\mathbf{U}_K = \mathbf{b}_3 \otimes \hat{\mathbf{n}}_3$
4. $\mathbf{U}_I - \mathbf{Q}_1\mathbf{Q}_2\mathbf{Q}_3\mathbf{U}_L = \mathbf{b}_4 \otimes \hat{\mathbf{n}}_4$
5. $\hat{\mathbf{n}}_1$, $\hat{\mathbf{n}}_2$, $\hat{\mathbf{n}}_3$ and $\hat{\mathbf{n}}_4$ lie on a plane

Parallelogram Martensite Microstructure

Star-lisclination

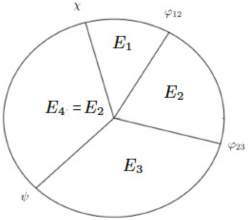

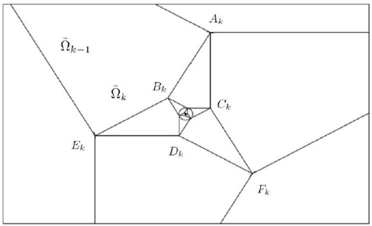

$\rightarrow$ Rigidity: solution is unique

S. Patching, P.C., A. Rueland
P.C., M. Porta, T. Lookman JMPS14

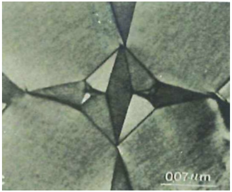

Acknowledgments

- JSPS Grant in Aid for Young Scientists B 2016-19
- European Research Council under the European Union's Seventh Framework Programme (FP7/2007- 2013) - ERC grant agreement N. 291053
- Department of Energy National Nuclear Security Administration under Award Number DE-FC52-08NA28613
- Prof. A. Planes and E. Vives research group
- LANL-work is unclassified

p.cesana@latrobe.edu.au